Capacitive detection of micrometric airborne particulate matter for solid-state personal air quality monitors

M. Carminati[1], L. Pedalà[1], E. Bianchi[2], F. Nason[2], G. Dubini[2], L. Cortelezzi[3], G. Ferrari[1], and M. Sampietro[1]

[1] *Dipartimento di Elettronica, Informazione e Bioingegneria, Politecnico di Milano, Italy*
[2] *Dipartimento di Chimica, Materiali e Ingegneria Chimica "Giulio Natta", Politecnico di Milano, Italy*
[3] *Department of Mechanical Engineering, McGill University, Canada*

Abstract:

A novel microsensor for capacitive detection of particulate matter (PM) directly in air is presented. The feasibility of detecting single PM_{10} particles (calibrated 10 μm polystyrene beads) by means of ad-hoc designed coplanar microelectrodes (4 μm gap), a PDMS air deposition system, and a low-noise (~2 aF capacitive resolution) readout electronics is experimentally demonstrated. Finite element numerical simulations have been performed to optimize the design of the microelectrodes, investigate the detection limit and validate the experimental results. The real-time deposition on the sensor surface of sequences of single industrial talc particles (average diameter of ~8 μm, corresponding to a signal of ~12 aF) has been successfully tracked with 10 ms temporal resolution and, subsequently, validated by microscope inspection. This CMOS- and MEMS-compatible capacitance detection technique enables radical miniaturization of next generation air quality monitors, paving the ways to their embedment in personal portable devices for pervasive mapping of air pollution.

Keywords: air pollution, portable dust monitoring, capacitive sensing, microelectrodes.

Corresponding Author:

Marco Carminati
Email: *marco1.carminati@polimi.it*
Phone: +39.02.2399.3773
Fax: +39.02.2399.3574
Politecnico di Milano, DEIB, Piazza Leonardo da Vinci, 32, 20133, Milano, Italy

1. Introduction

It has been widely demonstrated that there is a correlation between high concentrations of particulate matter (PM) in the atmosphere, mostly in urban environments, and the increase of some pathologies, in particular of pulmonary diseases [1-4]. Although the exposure to fine and ultrafine dust, among other air polluting agents, has been identified as a threat for human health (as well as for the environment and for cultural properties), several toxicological effects of inhaled micro and nanoparticles still need to be elucidated [5]. At the same time, the policies implemented to reduce PM emission, such as vehicular traffic restrictions, often have been shown to be ineffective [6]. This impasse is due to the complex and poorly understood dynamics that governs the generation and transport of PM. This process can be subdivided in three phases: (i) PM generation (in localized industrial plants such as mines, power generation plants and waste incinerators, as well as distributed sources among thousands of internal combustion vehicles and building heating systems) and release in the atmosphere, (ii) PM long range transport in the atmosphere, deposition and chemical contamination of the ground surfaces in relation to atmospheric activity, (iii) PM human exposure through inhalation (penetration in the lungs at different depths, according to the particle diameter [1]), and its toxic effects on the human body at various scales (molecular, cellular and tissutal). Although accurate models of these mechanisms are under investigation, advances are significantly hampered by the currently available monitoring instrumentation that lacks portability and appropriate spatio-temporal resolution [7-9]. Two are the main limitations of the current airborne dust analyzers [10]. On the one hand, several dust analyzers (such as the gravimetric ones [11] or real-time microbalances, based on mass-sensitive MEMS cantilevers, for micro [12] and nano-particles [13]) provide only the total mass of PM in a given volume of sampled air (for instance, 50 $\mu g/m^3$ of PM_{10}, as currently required by European regulations). They cannot measure the granulometry of PM (i.e. the distribution of particles sizes

usually divided into PM_{10}, $PM_{2.5}$ and PM_1 size classes) which is extremely relevant from a toxicological point of view. On the other hand, other systems based on laser scattering [14] or cascade of impactors with electrometers [15], while providing real-time detection and fast single particle analysis and granulometry, are too bulky (weight >1 kg) and expensive (>1000 $) to be capillary disseminated in a city. Therefore, the spatial resolution achievable with these devices is that allowed by only a few fixed (background stations) or movable sampling stations continuously operating in a metropolitan area.

Thus, motivated by the need to overcome such limitations, we devised a novel detection method based on a highly sensitive capacitive microsensor. In this article we demonstrate the feasibility of direct dielectric detection of single PM_{10} particles in air with the intent of paving the way to the development of highly miniaturized single particle (granulometric) detection devices. We believe that this impedance-based technique will eventually enable the embedment of solid-state air quality monitors in personal and networked mobile devices, such as smartphones, allowing radically new air monitoring strategies [5] based on real-time indoor and outdoor pervasive monitoring, personal dosimetry and participative pollution mapping.

2. Theory

2.1 Principle of detection

Our detection technique relies on the impedance variations measured by a pair of microelectrodes placed in the proximity of a stream of PM. The presence of a particle (replacing the equivalent fraction of air dielectric with its volume) interacts with the electric field lines and increases the capacitance between the electrodes because the relative permittivity of a particle is larger than that of air. A similar approach has been already validated for label-free counting and characterization of single biological cells (5-10 μm) and implemented on microfluidic platforms for impedance

flow cytometry [16] or for detection of metallic debris in lubricant oils [17]. In this article we present a similar, but more challenging, approach for the detection of PM in air. Note that humidity, in the form of micro water droplets (ε_r = 80), could generate miscounting as it happens in other in-air PM detection techniques (laser scattering and microbalance). This problem, however, can be easily solved by adding a pre-heating microchamber to the air sampling duct to force the evaporation of the airborne water droplets before they can reach the sensor.

Two in-liquid techniques for the detection of airborne particles have been proposed in literature, but they cannot be implemented in our case. The first technique has been developed only for particles of a given size (pollen ~330 nm) that were dispersed in a conductive liquid and transported through a size-tailored nano-channel (500 nm) with transversal microelectrodes, allowing contemporary ionic blockade and transversal current sensing [18]. The second technique leverages the condensation of water vapor on nanoparticles to increase their detectable diameter. In this way it is easier to count the particles, but it is more difficult to determine their size and, therefore, characterize the granulometry distribution [19].

Since our goal is to detect PM present in air, we decided to design a device able to characterize the distribution of microparticles directly in air. There are two main challenges. The particle transport is hard to implement because the density of air is much smaller than the density of the particles. The detection of particles is difficult because the dielectric contrast is small. It could be tempting to use a liquid buffer to overcome these difficulties. However, the price to be paid is high because dissolving the particles dispersed in air in a liquid is far from being trivial and the buffer liquid has to be highly purified and contained in a specifically designed water-tight reservoir. Therefore, this choice would make the design more complicated and harder to integrate in a portable device.

In the case of a highly conductive buffer liquid the conductivity contrast is high and, thus, the insulating particles can be detected measuring a large conductance decrease (current signal ΔI

~ -10 μA). In air, instead, the dielectric contrast is small and, thus, the capacity signal ΔC produced by a 10 μm particle is of the order of 10 aF, corresponding (at 1 MHz) to a signal $\Delta I \sim +60$ pA, i.e. about five orders of magnitude smaller than the corresponding measurement obtained using a buffer fluid. In order to resolve the tiny capacitance variations induced by nanoparticles in air, a specific design of the sensing electrodes is needed and will be presented in the next section.

2.2 Parallel versus coplanar electrode configuration

The architecture of the electrodes is crucial for optimizing the performance and operability of the sensor. Figure 1 shows the two main configurations (parallel and coplanar) conceivable for a solid-state sensor system. In the parallel-plate geometry (see Fig.1a) a stream of PM is forced to flow between the electrodes. The presence of a particle generates a capacitive jump (ΔC) whose amplitude is related to the diameter D and dielectric constant ε_r of the particle. However, due to the homogeneity of the electric field, the jump is independent of the vertical distance H of the particle from the electrodes. Note that the concurrent variability of D and ε_r might make ambiguous the determination of the particle size using a single ΔC measurement. However, this ambiguity can be substantially reduced by recalling that $\Delta C \sim D^3$ and $\Delta C \sim \varepsilon_r$, and combining in cascade or in parallel multiple sensors of different geometries. The same kind of ambiguity affects the instruments based on laser scattering detection, where the intensity of the scattered light depends on the particle diameter (as D^6 or D^2 depending on the diameter/wavelength ratio) and on its refraction index (whose distribution is ignored and an average value is assumed) [20]. The main limitation of the parallel-plate geometry is that it cannot be used for detecting particles having a wide range of sizes. In fact, the diameter of the largest particles determines the distance between the plates (with appropriate margins and input filters to prevent clogging), thus reducing

the magnitude of the sensor capacitance and its modulation ΔC, which are crucial for detecting the smallest particles.

The coplanar geometry (Fig. 1b) has several advantages over the parallel-plate geometry. First, the coplanar electrodes are easier to fabricate. Second, it permits detecting particles over a wide range of sizes with minimal risk of clogging. Third, this geometry permits operating the sensor in two different conditions: when the PM flows over the electrodes or when the PM sediments, by natural settling or forced deposition, over the electrodes. Note that the coplanar configuration allows us to take advantage of the non-negligible effect of gravity on the particles enabling significant relaxation of the detection speed requirements.

The motion of the particles with respect to the coplanar electrodes has, obviously, an impact on the shape of the signal to be detected. In the case when a stream of single particles flies over the electrodes, each particle generates a single positive pulse of amplitude ΔC and width Δt (determined by the flow rate), see Fig. 1d. Instead, in the deposition case, the capacitive signal results in a rising staircase corresponding to the progressive accumulation (integral) of the particles over the electrodes, see Fig. 1e. Note that in the latter case, a periodic cleaning of the sensor surface is required for prolonged measurements. This can be implemented by means of lateral air jets or surface acoustic waves, such as those employed in the sensor cleaning systems of digital cameras [21]. Finally, in order to cover a larger detection area the coplanar pair can be arranged in an interdigitated structure (Fig. 1c).

2.3 Numerical simulations for geometry optimization

The design of the electrodes and the optimization of their layout (inter-distance and size) have been performed with the support of finite-element simulations (COMSOL 4.3, "AC/DC Electrostatics" module). The spherical shape of the particles imposes a tridimensional simulation. However, the symmetry of the problem has been leveraged by simulating only a quarter of the full

domain (see inset of Fig. 2, the vertical symmetry planes intersect along the vertical axis of the particle), thus saving memory and improving accuracy. Assuming a differential excitation of the electrodes, the transversal symmetry plane is set to zero potential, while the electrode is defined as a port (biased at 1 V). The admittance to ground is then calculated by taking into account the symmetry of the half domain.

We have systematically estimated the amplitude of the capacitive jump ΔC, produced by the presence of a particle, as a function of the particle properties (diameter D and material relative permittivity ε_r), geometry of the electrodes and vertical distance of the particle from the electrodes H. Since border effects can be neglected for large electrodes, the ΔC induced by a single particle is independent of the electrode width W and therefore this dimension (100 μm in simulations, 3 mm in our prototype) will not be explicitly indicated hereafter. Figure 2 shows the capacitance increase ΔC_{FEM} as a function of the diameter of a spherical particle located in the middle of the electrodes. In the simulated geometry, as sketched in the inset of Figure 2, the electrodes are separated by a gap G = 2 μm (about the minimum gap achievable by lift-off lithography we have employed) and the particle is located at a fixed height H = 10 μm. The simulations confirm that ΔC_{FEM} decreases as D^3 (the particle volume). If we consider 1 aF as the best capacitive resolution achievable by a state-of-the-art instrument based on a discrete-component implementation [22], Figure 2 shows that PM_{10} can be robustly detected across the full range of dielectric constants, from ε_r = 2 to ε_r = 15. Note that the smallest detectable particle has a diameter of about 6 μm.

The dependence of ΔC_{FEM} on the design parameters (G, H and the electrode length L) has been also investigated. The reduction of the electrode gap (Fig. 3a) results in an increase of ΔC_{FEM} that, for example, doubles when G is reduced from 20 μm to 2 μm. Furthermore, as expected, the reduction of the vertical distance H of a particle from the electrodes improves the resolution of the measurements up to an order of magnitude (Fig. 3b).

The results of our FEM analysis suggest that the optimal design of a device able to detect the deposition of particles should have the minimum separation between the planar electrodes (i.e. minimum G achievable by the fabrication technology). Finally, our simulations show (Fig. 3c) that the optimal length L of the electrodes is 30 μm. Increasing the length is ineffective because the active field-lines are contained in a narrow band along the edge of the electrodes. As expected, for small values of ε_r, ΔC_{FEM} depends linearly on ε_r; while, when $\varepsilon_r > 15$, the effect tends to saturate (Fig. 3d) because an extremely polarizable particle tends to behave like a metal particle.

3. Experimental

3.1 Electrodes fabrication

Glass has been chosen as the best substrate material, instead of the more-commonly used silicon, in order to reduce the substrate-induced parasitic effects [23]. A 700 nm layer of resist AZ1512 was deposited on Pyrex wafers (525 μm thickness) by an EVG150 coater system (EVGgroup). UV patterned by means of a Chrome mask (5" Nanofilm SLM 5) on a Suss Ma6/Ba6, the photoresist layer was then developed on the same coater system. On an evaporator (Leybold optics, LAB600H) a 100 nm gold layer was deposited on a 20 nm titanium adhesive layer. The electrodes were then finalized in a lift-off bath and diced (Disco DAD321) to fit in the PCB chip holder.

3.2 Design of the electronic front-end

The sensor capacitance is measured by means of the synchronous detection architecture illustrated in Fig. 4: a sinusoidal voltage V_{AC} at frequency f_{AC} energizes one electrode and the capacitive current is collected at the other electrode, converted into a voltage by the custom-designed low-noise front-end and fed to a lock-in demodulator (HF2LI by Zurich Instruments). The analog circuit

consists of a transimpedance amplifier with capacitive feedback C_F of nominal value 1 pF (actual capacitance ~1.4 pF, comprising a 10% tolerance and additional 0.2 pF due to the 0805 SMD package), which is a noise-free component, providing a frequency-independent gain equal to -$C1/C_F$. A large 1 GΩ resistance was also inserted to reset the bias, without introducing a significant thermal white noise (4 fA/√Hz). The capacitance of the fabricated microelectrodes ranges from 0.1 pF (G = 10 μm) to 0.7 pF (G = 4 μm). These values mainly depend on the gap G, but they are also affected by the stray capacitance of the connections (i.e., by the length of the metal connections on the chip, which are dominating with respect to the short and distant external wirings). In order to maximize the *Signal-to-Noise Ratio* (SNR), the ADA4817 operational amplifier with JFET input was chosen because of its low equivalent voltage noise (4nV/√Hz), its low input capacitance (C_{IN} = 1.4 pF) and its low current noise (2.5 fA/√Hz). All these values provide a corner frequency sufficiently low so that the maximum SNR can be reached at frequencies below 10 MHz. Considering 1 pF of additional stray capacitance to ground (giving a total C_S ~3 pF), the measured noise spectrum (~20 nV/√Hz at 1 MHz) of the front-end matches the expected values. Thus, neglecting other noise sources (i.e. with an ideal lock-in generator), the expected capacitive resolution of the readout electronics would be extremely good (~1 aF with V_{AC} = 1 V, f_{AC} = 1 MHz, BW = 1 kHz, see Tab. 1) However, in the real conditions, due to the internal fluctuations affecting the reference voltage of the output digital-to-analog converter of the sinusoidal generator, the capacitive resolution performance results degraded by three orders of magnitude (see Tab. 1). Consequently , in order to circumvent the low-frequency instability of the sinusoidal voltage source of the lock-in system, a differential sensing configuration was necessarily adopted, by adding an inverting buffer (200 MHz bandwidth) to counter-driving a third electrodes. This differential configuration allows reducing the injected signal (about 25 times, and thus also the impact of the V_{AC} noise) in the virtual ground. Thanks to the difference between the two anti-symmetric paths

through *C1* and *C2*, and, in case of good matching (a 5% mismatch was experimentally found on the fabricated chips), allows nonetheless achieving a very low noise floor (~2 aF rms with *BW* = 1 Hz). In the presence of a particle, one sensor is unbalanced with respect to the other and the differential signal can be amplified and correctly detected.

3.3 Design of the fluidics

In order to induce the deposition of PM on the microelectrodes, an air conveyor system has been implemented. Gravity and the viscous drag induced by the forced air flow are considered as the dominating forces determining the PM trajectories. In fact, due to the large size of the particles, Brownian motion of the air molecules can be neglected. Electrostatic forces are usually also negligible due to the neutrality of the majority of the considered particles. Powder samples are loaded in an aerosol generator where a jet of pure air (filtered with a 0.2 μm HEPA filter) is forced by means of an external pump. A small fraction of the powder gets turbulently suspended in air and conveyed to the test chamber where the fluid dynamic field induces the dispersion of particle into a low density monolayer. A fluidic chamber (20 mm long, 9 mm wide and 200 μm high) was created in PDMS (Sylgard184 Dow Corning) and bonded to a glass slide hosting the microelectrodes and forming the bottom of the chamber. The chamber has a round inlet on the top, connected to a nozzle-shaped inlet tubing, and is open-ended to let air outflow. Single chambers as well as double chambers for differential detection have been fabricated (Fig. 5).

4. Results and discussion

4.1 Static detection of calibrated beads

Static tests have been preliminarily performed in order to experimentally prove the principle of capacitive detection of single microparticles in controlled and well defined conditions. Dry

monodispersed and certified polystyrene beads (ε_r = 2.6, by Thermo Scientific, USA) have been positioned across the gap between the electrodes and then removed by means of a tungsten tip, manually operated under the microscope. Capacitance was continuously measured during the following three phases. In the first phase, the electrodes free of particles and the baseline level (set by the mismatch between the differential pairs of electrodes in this case equal to ~14 fF) was recorded. In the second phase, a few beads were manually placed over the gap between the electrodes and the resulting increase of the capacitance was detected both for 20 µm (Fig. 6) and 10 µm (Fig. 7) diameters. In the third phase, the beads were removed and the capacitance returned to its initial value. Since these were static experiments, a 1 Hz lock-in bandwidth was chosen and V_{AC} = 1 V, resulting in a 1.16 aF rms resolution that grants a good SNR (>40). Measurements taken using particles of different diameters and gaps of different width matched very well the values obtained numerically. In the case of a single 20 µm bead (Fig.6) over a 10 µm gap the simulated ΔC_{FEM} is 42 aF. The measured ΔC = 73 aF is consistent with the presence of two beads, one perfectly centered on the gap and the other tangent to the electrode edge (Fig 6c), thus giving a ~30% smaller contribution. In the case of a single 10 µm bead (Fig.7) over a 4 µm gap the expected ΔC_{FEM} is 25 aF. The measured ΔC = 50 aF is consistent with the presence of a cluster of 4 particles, 2 of which are on the gap and two away from the gap (Fig. 7c).

4.2 Dynamic dust detection

Microtalc powder (Microtalc FC CG by Mondo Minerals, The Netherlands) has been chosen as a good PM_{10} model, thanks to its size distribution (a lognormal diameter distribution with a median of 8 µm), abundance, ease of manipulation and absence of environmental and health danger. The ε_r of this MgO-based talc powder is 2.4 (measured in a large parallel-plate fixture and consistent with the value reported in the literature [24]), i.e., very similar to the beads we have used in the static tests.

Initially, we performed a dynamic test connecting the talc aerosol generator with a single fluidic chamber placed above the differential electrodes (G = 4 μm). As reported in Fig. 8, the pump was activated for a few seconds and the deposition on the electrodes of a few talc microparticles on the electrodes has been clearly recorded (V_{AC} = 1 V). For these experiments, the detection bandwidth was set to 100 Hz (corresponding to a 3 aF rms resolution) that is suitable to track fast deposition events. In this configuration, the granularity (~10 aF steps) corresponding to the arrival of single particles is well apparent. During the deposition of the particles a non-monotonic signal was recorded because of the differential measurements between a triplet of adjacent and matched electrodes (as shown in Fig. 4). The landing of particles on C1 sensor produced positive jumps, while the deposition of PM on the adjacent C2 (negatively driven) produced negative jumps. After the pump was switched off (producing an electric spike that is visible also in lock-in output), the chamber was gently removed and the glass slide hosting the electrodes was placed under a microscope for visual inspection. Image processing was used to count the number of microparticles present over the gaps of the electrodes and then the total differential volume ΔVol_{final} of PM could be calculated. As reported in Fig. 8, there is a good quantitative agreement between the final capacitance variation ΔC_{final} and ΔVol_{final} (in spite of the inaccuracies due to the PM irregular shapes of the particles, approximated with spheres and ellipsoids, and due to the difficulty in extracting the thickness of talc fragments from microscope images, see Fig. 9). Figure 8c shows three consecutive negative jumps (-60 aF, -20 aF and -80 aF) corresponding to the deposition of three particles (two large and one small), whose presence was verified by microscope inspection (see inset).

Finally, in order to produce a monotonic increasing signal and, therefore, facilitate the interpretation of the results, a dual-chamber system was build and tested. A sealed dummy chamber hosting a second pair of differential electrodes (Fig. 5) was added to the detection system. As shown in Fig. 9, the deposition of single particles was clearly recorded. Figure 9a shows the signal

variation induced by a single particle α landing exactly between the electrodes (ΔC ~70 aF). Figure 9b shows the signal variation induced by the sequential arrival of three particles. The associated optical analysis of the electrode confirmed the presence of only three fragments: β is tangent to the gap (ΔC ~20 aF, D ~15 μm), γ is the biggest particle lying across the gap (ΔC ~80 aF, D ~25 μm) and δ, which covers the gap, is laterally displaced (ΔC ~50 aF, D ~20 μm). The slight increase in the noise level here observed is due to the higher mismatch affecting the sensor in the dual-chamber prototype. In fact, in order to accommodate the space for the wall separating the two chambers, the differential electrodes were no longer adjacent and the larger distance between them reduces their matching, thus allowing the generator noise to slightly worsen the resolution (~7.5 aF rms). In a further optimized prototype this deficiency can be easily overcome and the best resolution of 3 aF over a 100 Hz bandwidth as in Fig. 8 can still be reached (see Tab. 1).

4.3 Performance summary and comparison

The continuous operating time t_{op} of the sensor, i.e. the interval up to when cleaning the electrodes surface becomes necessary, can be easily estimated. Considering a total sensing area given by the electrode length multiplied by 3G (the gap + one band of width G along both electrodes edges), the maximum number of particles covering this area is ~460. Since in Milan, a highly polluted city, the maximum concentration of PM_{10} is reported to be ~0.1 cm^{-3} [25], with the currently-adopted input flow rate of 0.45 l/min, the minimum time required to completely fill the electrode surface with a single layer of particles is about 10 minutes. This value appears reasonable with respect to a cleaning time expected to be in the range of a few seconds. However, if necessary, t_{op} can be further increased by increasing the sensor area (for instance, a 1 mm by 1 mm area would correspond to t_{op} = 5 hours) or by reducing the aspiration flow rate.

Although an efficient solution for periodic cleaning is crucial for the practical realization of a complete miniaturized instrument, this need is common to other emerging solid-state PM detection technologies, in particular those based on micro and nano resonating cantilevers [26-27]. Thus, the development of such a cleaning solution will benefit from similar efforts carried out for competing (and possibly complementary) microscale technologies. A comparison between the proposed technique and other MEMS-compatible technologies for micro and nanoparticles detection is summarized in Tab. 2.

Finally, it should be noted that this technique is not able to discriminate between a single large particle and a cluster of smaller particles having the same equivalent volume. The same limitation, however, affects all the other technologies mentioned above, either based on laser scattering (volume sensitive) or on micromechanical resonators (mass sensitive). In commercial state-of-the-art optical instruments the risk of artifacts in granulometric spectra due to agglomerates is mitigated by focusing PM into a single stream. Consequently, it can be envisioned that solutions based on fluid dynamic focusing or turbulent agitation of PM samples can reduce this risk of altered counts due to particles clustering down to a statistically irrelevant level. Separation approaches based on inertial forces are expected to be more effective for larger particles (PM_{10}) due to the larger mass. Separating clusters of smaller particles (such PM_1 and below) appears extremely challenging due to the larger surface-to-volume ratio and, thus, to the prevalence of adhesion forces with respect to inertial ones.

5. Conclusions

We have presented a novel electric technique for direct detection and discrimination of PM in air. We have successfully demonstrated the capability to resolve single PM_{10} by means of capacitance measurements between coplanar microelectrodes (gaps of 4 μm and 10 μm), both statically (with calibrated 10 μm and 20 μm polystyrene beads), and dynamically (with air-conveyed 8 μm talc

particles). A low-noise front-end based on capacitive feedback, combined with a differential configuration (to reduce the impact of the V_{AC} generator noise) allowed achieving a suitable resolution (~1.2 aF). The correspondence between the measured capacitance variations (tens of aF) and the particle volume (of a homogeneous known material) has been validated by means of finite element simulations (used to optimize the electrode layout) and optical microscopy. For the purpose of granulometry, the uncertainty due to the unknown distribution of actual dielectric constants with respect to the assumption of an average $\varepsilon_{r\text{-}mean}$ can be mitigated by using electrodes with varying gaps, leveraging the different scaling laws (cubic vs. linear). Our technique can be further improved by designing a new set of electrodes arranged in a serpentine-shaped interdigitated configuration, in order to uniformly cover a larger detection area and, thus, avoid the uncertainty due to the landing position.

In order to detect smaller particles ($PM_{2.5}$, PM_1 and sub-micrometric particles) of greater toxicological relevance, an integrated microelectronic technology can be adopted for the realization of a single chip hosting the planar microelectrodes (fabricated on the highest metal layer, exposed to the air, and separated by sub-micrometric gaps) on top of the analog front-end, thus placed extremely close to the electrodes for radical minimization of the stray capacitance. To this end, we can leverage the improved capacitance resolution (zeptoFarad [28]) that we have previously demonstrated with a low-noise CMOS amplifier, in order to detect PM_1. Aside from being very promising for ultrafine PM detection in air, this envisioned monolithic single-chip realization fosters a significant miniaturization of the system (few mm^3) and, thus, paves the way to its MEMS-like integration inside personal portable smart devices for continuous and capillary air monitoring.

Acknowledgments

Fondazione CARIPLO (Milano, Italy) is gratefully acknowledged for financing this work under project MINUTE (grant no. 2011-2118). Federico Pedersini is thanked for providing a sample of talc powder. The authors would like to acknowledge also the Centre of MicroNanotechnology (CMi) at École Polytechnique Fédérale de Lausanne for its support and help concerning fabrication issues.

References

[1] A. Seaton, W. MacNee, K. Donaldson, D. Godden, Particulate air pollution and acute health effects, *Lancet* 345 (1995) 176-178.

[2] N. Kunzli, R. Kaiser, S. Medina, M. Studnicka, O. Chanel, P. Filliger, M. Herry, F. Horak, Public impact of outdoor and traffic-related air pollution: a european assessment, *Lancet* 356 (2000) 795-801.

[3] O. Raaschou-Nielsen, *et al.*, Air pollution and lung cancer incidence in 17 european cohorts: prospective analyses from the european study of cohorts for air pollution effects (ESCAPE), *Lancet Oncology* 14 (2013) 813-822.

[4] F. Farina, G. Sancini, C. Battaglia, V. Tinaglia, P. Mantecca, M. Camatini, P. Palestini, Milano summer particulate matter (PM10) triggers lung inflammation and extra pulmonary adverse events in mice, *PLoS One* 8 (2013) e56636.

[5] T.A.J. Kuhlbusch, U. Quass, G. Fuller, M. Viana, X. Querol, K. Katsouyanni, and P. Quincey, Air pollution monitoring strategies and technologies for urban areas. *Urban Air Quality in Europe, Handbook Env. Chem.* 26 (2013) 277-296.

[6] K.H. Kim, Z.H. Shon, Long-term changes in PM10 levels in urban air in relation with air quality control efforts, *Atm. Environ.* 45 (2011) 3309-3317.

[7] G. Lonati, S. Ozgen, G. Ripamonti, S. Cernuschi, M. Giugliano, Pedestrian exposure to size-resolved particles in Milano. *J. Air Waste Manage. Assoc.* 61 (2011) 1273-1280.

[8] V. Bernardoni, R. Vecchi, G. Valli, A. Piazzalunga, P. Fermo, PM10 source apportionment in Milan (Italy) using time-resolved data, *Sci. Total Environ.* 409 (2011) 4788-4795.

[9] L.M. Zwack, C.J. Paciorek, J.D. Spengler, J.I. Levy, Characterizing local traffic contributions to particulate air pollution in street canyons using mobile monitoring techniques, *Atm. Environ.* 45 (2011) 2507-2514.

[10] M. Carminati, M. Sampietro, G. Carminati, Analysis of instrumentation performance for distributed real-time air quality monitoring, *Proc. IEEE Workshop on Environmental Energy and Structural Monitoring Systems* (2011) 28-33.

[11] K.R. Spurny, Methods of aerosol measurement before the1960s. *Aerosol Sci. Technol.* 29 (1998) 329-349.

[12] I. Paprotny, *et. al.*, Microfabricated air-microfluidic sensor for personal monitoring of airborne particulate matter: design, fabrication, and experimental results, *Sens. Act. A* (2013) 506-516.

[13] H. S. Wasisto, S. Merzsch, A. Waag, E. Uhde, T. Salthammer, E. Peiner, Portable cantilever-based airborne nanoparticle detector, *Sens. Act. B* 187 (2013) 118-127.

[14] J.K. Agarwal and G.J. Sem, Continuous flow, single-particle-counting condensation nucleus counter, *J. Aerosol Sci.* 11 (1980) 343-357.

[15] J. Keskinen, K. Pietarinen, M. Lehtimäki, Electrical low pressure impactor, *J. Aerosol Sci.* 23 (1992) 353-360.

[16] T. Sun, H. Morgan, Single-cell microfluidic impedance cytometry: a review, *Microfluid. Nanofluid.* 8 (2010) 423-443.

[17] L. Du, J. Zhe, J. Carletta, R. Veillette, F. Choy, Real-time monitoring of wear debris in lubrication oil using a microfluidic inductive coulter counting device, *Microfluid. Nanofluid.* 9 (2010)1241-1245.

[18] C. Kawaguchi, T. Noda, M. Tsutsui, M. Taniguchi, S. Kawano, T. Kawaii, Electrical detection of single pollen allergen particles using electrode-embedded microchannels, *J. Phys.: Condens. Matter* 24 (2012) 164202/1-6.

[19] I. Iskra, A. Detela, M. Viršek, V. Nemanic, D. Križaj, D. Golob, J. T.van Elteren, M. Remškar, Capacitive-type counter of nanoparticles in air, *Appl. Phys. Lett.* 96 (2010) 093504/1-3.

[20] W. C. Hinds, Aerosol Technology, 2nd ed., John Wiley and Sons, New York, 1999.

[21] G. Brereton, Q. Qi, Mechanisms of removal of micron-sized particles by high-frequency ultrasonic waves, *IEEE Trans. Ultrason. Ferroelectr. Freq. Control* 42 (1995) 619-629.

[22] M. Carminati, G. Ferrari and M. Sampietro, AttoFarad resolution potentiostat for electrochemical measurements on nanoscale biomolecular interfacial systems, *Rev. Sci. Instrum.* 80 (2009) 124701/1-10.

[23] M. Carminati, M. Vergani, G. Ferrari, L. Caranzi, M. Caironi, M. Sampietro, Accuracy and resolution limits in quartz and silicon substrates with microelectrodes for electrochemical biosensors, *Sens. Act. B* 174 (2012) 168-175.

[24] A. Kirak, H. Yilmaz, S. Güler, Ç. Güler, Dielectric properties and electric conductivity of talc and doped talc, *J. Phys. D: Appl. Phys.* 32 (1999) 1919-1927.

[25] G. Lonati, M. Giugliano, Size distribution of atmospheric particulate matter at traffic exposed sites in the urban area of Milan (Italy), *Atm. Environ.* 40 (2006) 264-274.

[26] A. Hajjam, J.C. Wilson, S. Pourkamali, Individual air-borne particle mass measurement using high-frequency micromechanical resonators, *IEEE Sens. J.* 11 (2011) 2883-2890.

[27] H.S. Wasisto, S. Merzsch, A. Stranz, A. Waag, E. Uhde, T. Salthammer, E. Peiner, Silicon resonant nanopillar sensors for airborne titanium dioxide engineered nanoparticle mass detection. *Sens. Act. B* 189 (2013) 146-156.

[28] M. Carminati, G. Ferrari, F. Guagliardo, M. Sampietro, ZeptoFarad capacitance detection with a miniaturized CMOS current front-end for nanoscale sensors, *Sens. Act. A* 172 (2011) 117-123.

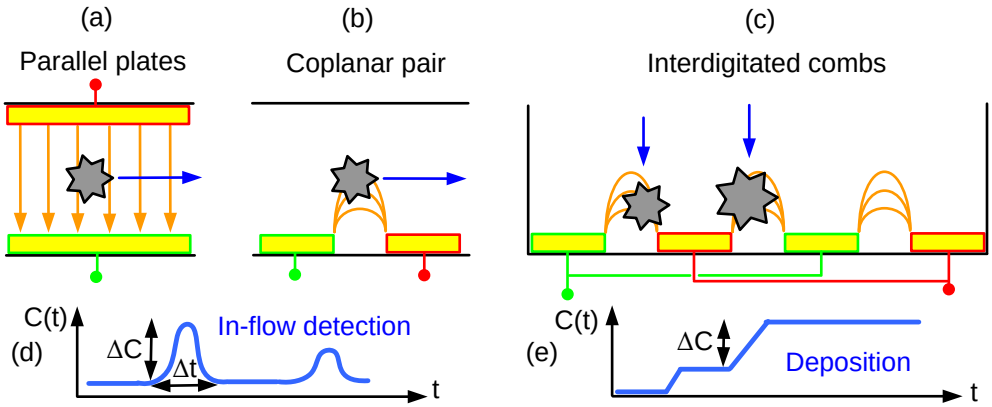

Fig. 1 Possible configurations of the proposed solid-state direct capacitive sensor of PM in air: (a) parallel-plate microelectrodes for in-flow detection of PM, (b) single coplanar pair of electrodes and (c) multiple interdigitated electrodes, an extension of (b), to cover a larger deposition area. The latter are suitable for both stream flow (d) and deposition (e) detection.

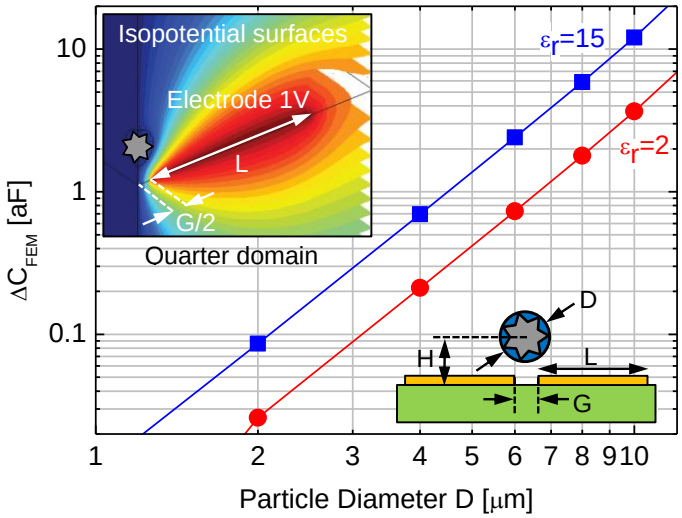

Fig. 2 Simulated capacitance increase due to the presence of a single spherical particle of diameter D and relative permittivity ε_r located at a height H = 10 μm over the center of the gap G = 2 μm between the electrodes. Thanks to the symmetry of the 3D domain, only a quarter of the volume is simulated in COMSOL (inset, colorbar from 0 to 1 V potential).

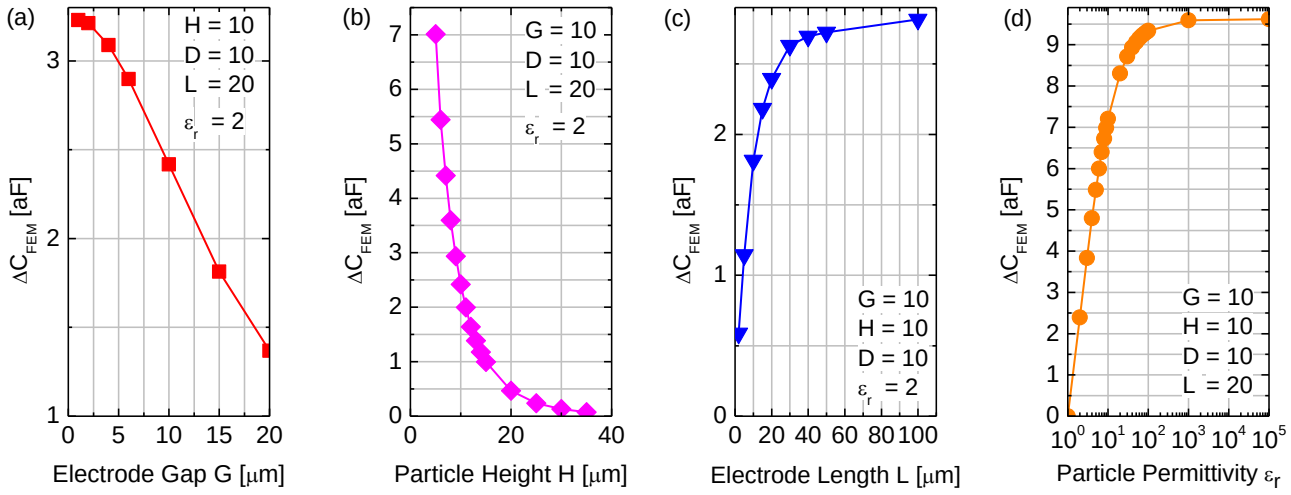

Fig. 3 Simulated dependence of ΔC_{FEM} on the gap G between the electrodes (a), on the vertical distance H of the centroid of a PM_{10} particle from the bottom electrode level (b), on the electrode longitudinal length L (c) and on the particle relative dielectric constant ε_r (d).

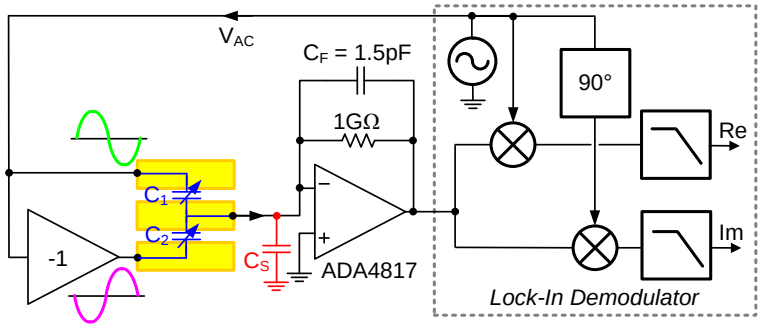

Fig. 4 Scheme of the capacitance sensing circuit comprising a low-noise integrator front-end and synchronous lock-in detector connected to a triplet of electrodes operated in differential mode. Note that for single-ended measurement the inverting buffer is disabled.

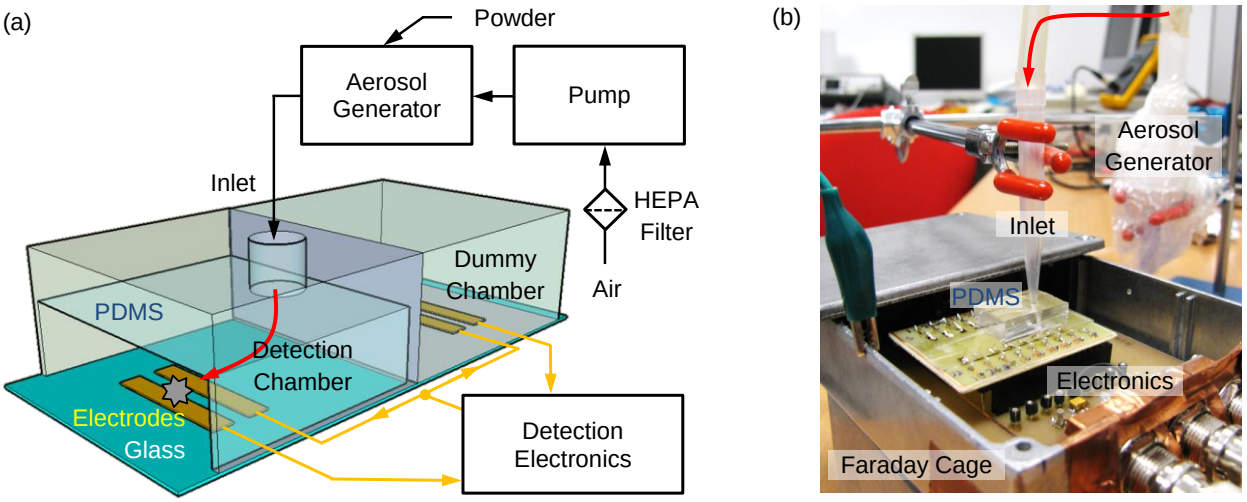

Fig. 5 (a) Sensor differential arrangement with a double PDMS chamber allowing the deposition of PM only on top of a single pair of microelectrodes (thus providing a monotonic signal). The solid aerosol is created loading the test powder in a highly turbulent separate chamber driven by an external pump fed with filtered air. (b) Photograph of the experimental setup for prototype characterization: the chip is mounted on an interchangeable board, inserted in the motherboard hosting the front-end electronics in a grounded Faraday Cage.

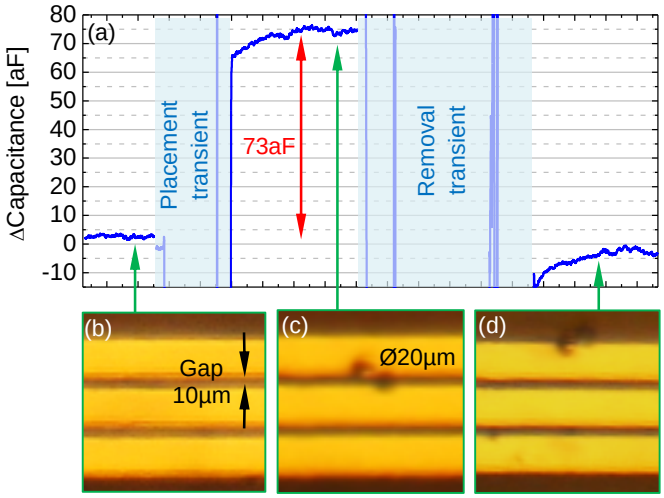

Fig. 6 Static detection of two polystyrene particles of 20 µm of diameter producing a capacitance increase of 73 aF (the noise floor is 1.16 aF rms with V_{AC} = 1V, BW = 1Hz) on a differential triplet of electrodes with a gap G =10 µm.

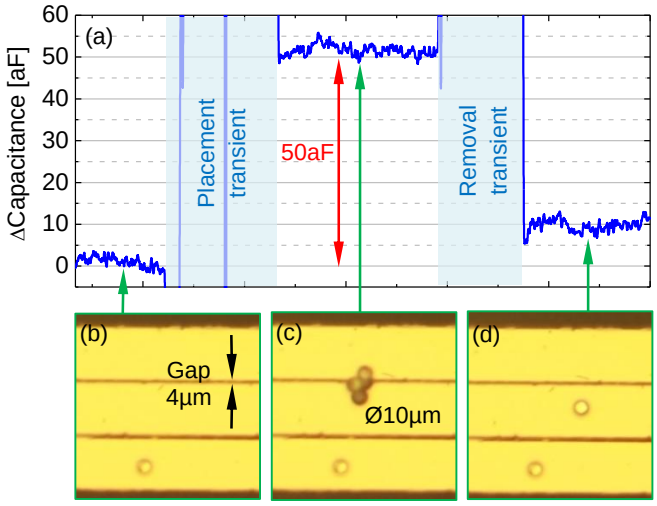

Fig. 7 Static detection of two polystyrene particles of 10 µm of diameter producing a capacitance increase of 50 aF on a differential triplet of electrodes with a gap G = 4µm.

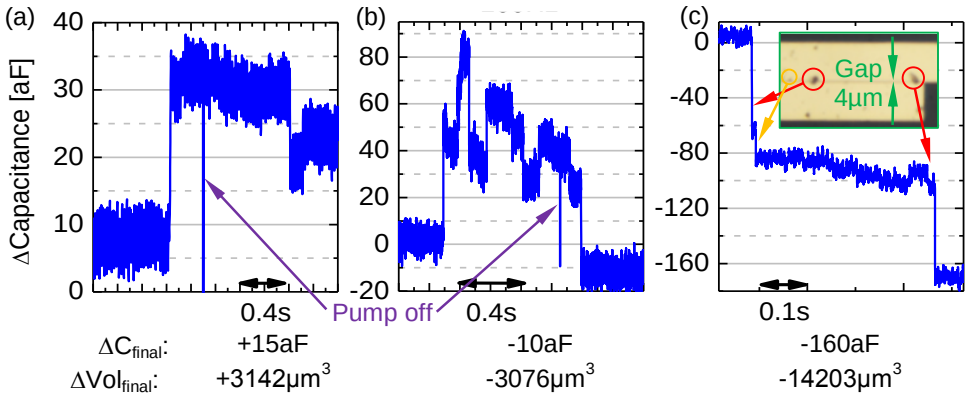

Fig. 8 Dynamic detection (with *BW* =100 Hz) of different sequences of a few talc microparticles depositing on a differential triplet of electrodes in a single chamber. In the three experiments reported here, the total measured capacitance variation ΔC_{final} is in agreement with the optical assessment of the number and size of the deposited particles and gives an estimate of the total volume occupied by the particles (negative sign corresponding to C2 > C1).

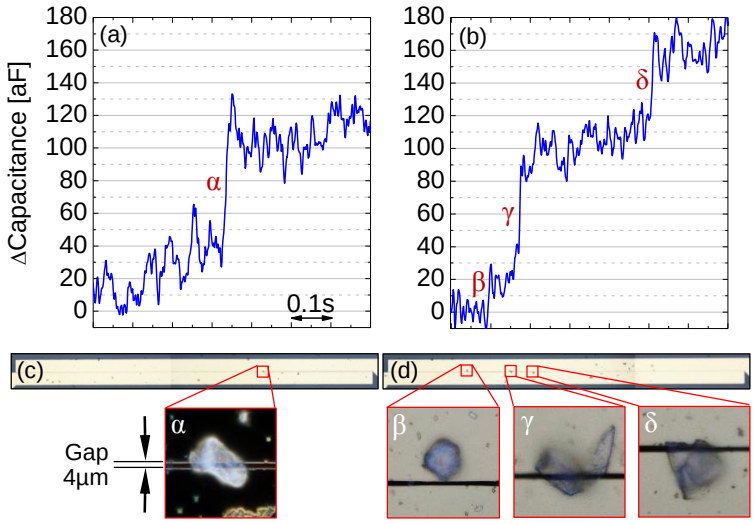

Fig. 9 Detection of the deposition of single talc microparticles by means of a differential configuration (employing two separate pairs of electrodes) covered with a double-chamber fluidic system, allowing monotonic sensor response (V_{AC} = 1V, BW = 100 Hz, 7.5 aF rms noise floor).

Tab. 1 Summary of sensor RMS capacitive noise levels (i.e. achievable resolution) measured in different operating conditions and for different lock-in averaging bandwidths (BW).

Measured noise in the following conditions (f_{AC} = 1MHz, V_{AC} = 1V)	**RMS Noise (BW = 1 Hz)**	**RMS Noise (BW = 100 Hz)**	**RMS Noise (BW = 1 kHz)**
Front-end only (ideal lock-in)	31 zF	0.3 aF	1 aF
Complete system, single-ended electrodes	30 aF	-	-
Complete system, differential (good matching)	1.16 aF	3.3 aF	5 aF
Complete system, differential (worse matching)	-	7.5 aF	-

Tab. 2 Comparison of our approach with other solid-state and MEMS-compatible PM detection technologies recently proposed in the literature. As a reference, the classic gravimetric technique and laser scattering technology are also reported.

Technology	**Detection type**	**Particles diameter range**	**Single particle resolution**	**Advantages**	**Drawbacks**
Standard gravimetric filters	Mass	0.2 μm - 50 μm	No	Legislation reference	Off-line, no granulometry
Resonating nanopillar [27]	Mass	0.125 μm - 2 μm	Yes	High resolution	Requires cleaning
IBAR resonator [26]	Mass	0.2 μm - 1 μm	Yes	Good resolution	Requires cleaning
FBAR resonator [12]	Mass	$PM_{2.5}$	No	Virtual impactor	No granulometry
Laser scattering	Volume, n	0.3 μm - 30 μm	Yes	Wide detection range	Size, cost
Capacitive detection (this work)	Volume, ε_r	6 μm - 30 μm	Yes	Simple, miniaturized	Requires cleaning

Highlights:

- Capacitive detection of single dust particles in air is proposed
- FEM simulations are used to optimize the design of coplanar microelectrodes
- Sensor design including attoFarad resolution electronics and fluidics is described
- Static detection of 10 and 20 μm polystyrene beads is achieved
- Dynamic detection of 8 μm talc microparticles dispersed in air is reported

This is an Accepted Manuscript article of an article published By Elsevier in Sensors and Actuators A: Physical, Volume 219, 1 November 2014, Pages 80-87.